The authors wish to express their gratitude to Professor H. Iwasaki, Institute of High Energy Physics, and Professor T. Sakurai, Institute for Materials Research, Tohoku University, for their continuous encouragement throughout the present investigation. Dr Yamamoto, National Institute for Research in Inorganic Materials, has kindly permitted the authors to use his program *REMOS* for the present study.

References

BUDKOWSKI, A., MARINKOVIC, V., PRODAN, A. & BOSWELL, F. W. (1990). *Phys. Status Solidi A*, **117**, 351–362.
GUNZEL, E. & SCHUBERT, K. (1958). *Z. Metallkd.* **49**, 124–133.
HANSEN, M. (1958). *Constitution of Binary Alloys*, pp. 622–628. New York: McGraw-Hill.
HIRABAYASHI, M., HIRAGA, K. & SHINDO, D. (1981). *J. Appl. Cryst.* **14**, 169–177.
HIRABAYASHI, M., YAMAGUCHI, S., HIRAGA, K., INO, N., SATO H. & TOTH, R. S. (1970). *J. Phys. Chem. Solids*, **31**, 77–94.
JANNER, A., JANSSEN, T. & DE WOLFF, P. M. (1983). *Acta Cryst.* A**39**, 658–666.
JANSSEN, T. & JANNER, A. (1987). *Adv. Phys.* **36**, 519–624.
KATAOKA, M. & IWASAKI, H. (1981). *J. Phys. F*, **11**, 1545–1556.
OKAMURA, K., IWASAKI, H. & OGAWA, S. (1968). *J. Phys. Soc. Jpn*, **24**, 569–579.
ONOZUKA, T., KAKEHASHI, S., TAKAHASHI, T. & HIRABAYASHI, M. (1989). *J. Appl. Cryst.* **22**, 272–282.
STEURER, W. (1989). *Phase Transit.* **16–17**, 103–118.
WATANABE, Y. & IWASAKI, H. (1982). *J. Appl. Cryst.* **15**, 174–181.
YAMAGUCHI, S. & HIRABAYASHI, M. (1972). *J. Phys. Soc. Jpn*, **33**, 708–716.
YAMAMOTO, A. (1983). *Acta Cryst.* B**39**, 17–20.

Acta Cryst. (1993). B**49**, 661–675

The Structure of Decagonal $Al_{70}Ni_{15}Co_{15}$

BY W. STEURER, T. HAIBACH AND B. ZHANG

Institut für Mineralogie der Universität, Welfengarten 1, *D*-3000 *Hannover* 1, *Germany*

S. KEK

Fachrichtung Kristallographie, Universität des Saarlands, D-6600 *Saarbrücken* 11, *Germany*

AND R. LÜCK

Institut für Werkstoffwissenschaft, MPI für Metallforschung, Seestrasse 75, *D*-7000 *Stuttgart* 1, *Germany*

(*Received* 11 *December* 1992; *accepted* 25 *March* 1993)

Abstract

The quasiperiodic structure of decagonal $Al_{70}Ni_{15}Co_{15}$ was determined on the basis of X-ray single-crystal intensity data using the *n*-dimensional embedding method. Centrosymmetric five-dimensional space group $P10_5/mmc$, three-dimensional reciprocal and direct quasilattice parameters: $a_i^* = 0.2636\ (1)\ Å^{-1}$, $i = 1,\ldots, 4$, $a_5^* = 0.24506\ (3)\ Å^{-1}$, $a_i = 3.794\ (1)\ Å$, $i = 1,\ldots, 4$, $a_5 = 4.0807\ (3)\ Å$. Five-dimensional unit-cell parameters: $d_i = 3.393\ (1)$, $d_5 = 4.0807\ (3)\ Å$, $\alpha_{ij} = 60°$, $\alpha_{i5} = 90°$, $i, j = 1,\ldots, 4$, $V = 302.4\ Å^5$, $M_r = 36.54$, $D_x = 4.5\ Mg\ m^{-3}$, $\mu = 10.1\ mm^{-1}$, Mo $K\alpha$, $wR = 0.078$, $R = 0.091$ for 253 unique reflections and 21 variables. A five-dimensional structure model was obtained by Patterson syntheses and refined by the least-squares technique. High-resolution electron-density maps were calculated by the maximum-entropy method. The structure is formally built up by two quasiperiodic atomic layers with stacking sequence *Aa* (*a* denotes the layer *A* rotated around $2\pi/10$). It is essentially isotypic to that of decagonal $Al_{65}Cu_{20}Co_{15}$ and shows locally a close resemblance to monoclinic $Al_{13}Co_4$. Columnar clusters parallel to the local tenfold screw axes, formed by ten pentagonal antiprismatic columns surrounding a central column, are found to be the basic structural building elements. Quasiperiodicity is forced by the formation of interconnected networks of closed icosagonal rings of pentagonal and rectangular structure motifs.

Introduction

Decagonal quasicrystals represent interesting intermediate states between icosahedral and crystalline phases with anisotropic physical and mechanical properties. The stable decagonal phase $Al_{70}Ni_{15}Co_{15}$, with needle-like decagonal prismatic morphology, was first synthesized by Tsai, Inoue & Masumoto (1989) by slow solidification. Its stability range between 773 K and the melting point was studied by Kek (1991). Other stable decagonal phases were found in the systems Al–Cu–Co by He,

Zhang, Wu & Kuo (1988), in Al-Cu-Rh and Al-Ni-Rh by Inoue, Tsai & Masumoto (1990), and in Al-Pd-Me with Me = Mn, Fe, Ru and Os by Beeli, Nissen & Robadey (1991) and by Tsai, Inoue & Masumoto (1991). The first quantitative *n*-dimensional structure analyses of decagonal phases were carried out for Al-Cu-Co by Steurer & Kuo (1990) [in the following referred to as paper (I)], for Al-Ni-Co by Yamamoto, Kato, Shibuya & Takeuchi (1990), for Al-Mn by Steurer (1991) and for Al-Mn-Pd by Steurer (1993). A structural study of Al-Ni-Co using high-resolution transmission electron microscopy (HRTEM) was performed by Hiraga, Lincoln & Sun (1991); the results of an electron-diffraction investigation of decagonal and approximant phases in the system Al-Ni-Co were reported by Edagawa, Ichihara, Suzuki & Takeuchi (1992*a*,*b*); high-order Laue-zone (HOLZ) patterns of decagonal Al-Ni-Co were discussed by Yan, Wang, Gui, Dai & He (1992). Besides this small number of experimental structural papers on decagonal Al-Ni-Co many theoretical studies have been published: Kang & Dubois (1993), Daulton & Kelton (1992), Song & Ryba (1992), Burkov (1991), to quote only a few, based mostly on the same sparse experimentally based knowledge about isotypic decagonal Al-Cu-Co-(Si). For a short review of the current models of decagonal structures see Henley (1993). The purpose of the present work was to obtain quantitative information about the structure of decagonal Al-Ni-Co in greater detail and based on more reliable experimental data than in the studies published previously.

Problems of quasicrystal structure analysis

Symmetry and metrics

The present structure analysis was carried out using the *n*-dimensional embedding method (*cf.* Janssen, 1988). The assignment of three-dimensional reciprocal basis vectors $\mathbf{a}_i^*$, the indexing of reflections and the embedding was performed in the same way as described in paper (I) for decagonal $Al_{65}Cu_{20}Co_{15}$. Thus, only a short summary is given here: the five-dimensional embedding space $\mathbf{V} = (\mathbf{V}^{\parallel}, \mathbf{V}^{\perp})$ consists of two orthogonal subspaces, the three-dimensional physical (parallel, external) space $\mathbf{V}^{\parallel}$ with basis vectors $\mathbf{v}_1$, $\mathbf{v}_2$, $\mathbf{v}_3$ and the two-dimensional perpendicular (complementary, internal) space $\mathbf{V}^{\perp}$ with basis vectors $\mathbf{v}_4$, $\mathbf{v}_5$. All physical-space reciprocal lattice vectors $\mathbf{H}^{\parallel} = h^{\parallel}_1\mathbf{a}'^*_1 + h^{\parallel}_2\mathbf{a}'^*_2 + h^{\parallel}_3\mathbf{a}'^*_3 = h_1\mathbf{a}_1^* + h_2\mathbf{a}_2^* + h_3\mathbf{a}_3^* + h_4\mathbf{a}_4^* + h_5\mathbf{a}_5^*$, with $h^{\parallel}_1$, $h^{\parallel}_2$ irrational and $h^{\parallel}_3$, h_i, $i = 1,\ldots, 5$, integer numbers, can be written as linear combinations of the five reciprocal basis vectors $\mathbf{a}_i^* = a_i^*(\cos 2\pi i/5, \sin 2\pi i/5, 0)$ with $i = 1,\ldots, 4$ and $\mathbf{a}_5^* = a_5^*(001)$. The star of these five reciprocal-basis vectors corresponds to a projection of the hypothetical five-dimensional reciprocal basis vectors $\mathbf{d}_i^* = (\mathbf{a}_i^*, 0, \mathbf{a}_{3i}^*)$, $i = 1,\ldots, 4$, $\mathbf{d}_5^* = (0, \mathbf{a}_5^*, 0)$ upon $\mathbf{V}^{\parallel}$. The direct-basis vectors (in the following called **d** basis), spanning the unit cell in five-dimensional space, can be written in the form $\mathbf{d}_i = 2/(5a_i^*)(\cos 2\pi i/5 - 1, \sin 2\pi i/5, 0, \cos 6\pi i/5 - 1, \sin 6\pi i/5)$, $i = 1,\ldots, 4$ and $\mathbf{d}_5 = 1/a_5^*(00100)$; the vector components refer to the above-mentioned five-dimensional orthogonal coordinate system spanned by the basis vectors $\mathbf{v}_i$, $i = 1,\ldots, 5$ (in the following called **v** basis). The absolute values of the vectors $\mathbf{d}_i^*$, $\mathbf{d}_i$ amount to $d_i^* = 2^{1/2}a_i^*$, $i = 1,\ldots, 4$, $d_5^* = a_5^*$, and $d_i = 2/(5^{1/2}a_i^*)$, $i = 1,\ldots, 4$, $d_5 = 1/a_5^*$, respectively. The *n*-dimensional least-squares structure refinements were performed on the **d** basis, the MEM calculations and the representation of the plots on the **v** basis.

Data set

Mostly because of the poor quality of the single crystals, especially in the case of decagonal phases, quasicrystal structure refinements do not give final *R* factors near 0.01 for complete data sets. Since the crystal quality and the eventual formation of microdomains or twins depends strongly on the conditions of crystal growth and thermal treatment (*cf.* Grushko, 1993, and references therein), quasicrystals of different origin and history may lead to different structure analysis results. Consequently, a detailed characterization of the crystals used, comprising diffraction patterns, should always be given in structural papers when phase diagrams are not known accurately.

What is the actual definition of a full data set in the case of quasicrystals with reflections densely filling the reciprocal space leading to an infinite number of reflections in the usual data-collection range $0 \le \sin\theta/\lambda \le 0.7$ Å^{-1}, corresponding to $|\mathbf{H}| = 2\sin\theta/\lambda = 1.4$ Å^{-1}? A simple answer can be given in terms of the *n*-dimensional description of quasiperiodic structures: the limiting sphere in three-dimensional reciprocal space is replaced by a hypersphere in *n*-dimensional reciprocal space with radius $|\mathbf{H}| = 1.4$ Å^{-1} (**H** now being an *n*-dimensional reciprocal-lattice vector). Such a data set warrants a well defined isotropic resolution function in all directions of the *n*-dimensional direct space comparable to that obtained in conventional structure analysis.

Twinning

For any diffraction study, it is essential to know whether the measured intensity data stem from a coherently scattering single crystal or from coherently or incoherently scattering twin individuals. The problems which arise during structure analyses of twinned crystals are well known from conventional structure determinations (*cf.* Araki, 1991, and references therein). The appearance of electron-diffraction patterns with tenfold rotational symmetry taken from twinned crystalline samples was demonstrated, for instance, by Song, Wang & Ryba (1991) and Fung, Zou & Yang (1987). In these cases, each single diffraction pattern of five or ten incoherently

scattering crystalline twin individuals can basically be identified, merohedral twinning is not possible. The test for incoherent twinning may become quite simple: our sample of $Al_{70}Ni_{15}Co_{15}$ shows systematically absent Bragg reflections (Fig. 1) of the type

$$h_1h_2\bar{h}_2\bar{h}_1h_5\text{: } h_5 = 2n + 1, \quad (0000h_5\text{: } h_5 = 2n + 1)$$

indicating *c*-glide planes and a 10_5-screw axis leading to the five-dimensional superspace groups $P10_5mc$ and $P10_5/mmc$, respectively (Rabson, Mermin, Rokhsar & Wright, 1991). This information rules out the case of incoherent twinning, since by superposition of the five or ten diffraction patterns of the respective twin individuals systematic absences with tenfold symmetry can never be obtained. One cannot exclude, however, pseudo-merohedral twinning of high-order approximants which also show a pseudo-decagonal diffraction symmetry with pseudo-extinction rules. Since it is known from high-temperature studies (Hiraga, Lincoln & Sun, 1991) that single grains of decagonal Al-Ni-Co give electron-diffraction patterns with diffraction symmetry $10mm$ and the systematic absences mentioned above, the intensity distribution of merohedrally twinned high-order approximants would be quite similar to that of the decagonal phase. Consequently, even a structure analysis assuming that such a twin data set was that of a decagonal phase would yield an acceptable structure model of the decagonal phase.

Microdomain structures, approximants

How would the results of our *n*-dimensional structure analysis be biased if the sample used were in fact a high-order rational approximant or a kind of crystalline microdomain structure with average pseudo-tenfold symmetry? The X-ray precession, cone-axis and Laue photographs of decagonal $Al_{70}Ni_{15}Co_{15}$ (Fig. 1) as well as four-circle diffractometer data show that the Bragg reflections are as sharp as those of metal crystals within our experimental resolution of about 0.002 $Å^{-1}$. Deviations from $10/mmm$ diffraction symmetry are not observable [the angle between $\mathbf{a}_i^*$ and $\mathbf{a}_{i+1}^*$ amounts to 72.00 (2)°]. These facts would be consistent with diffraction from perfect quasicrystals, high-order approximants in the form of single crystals or pseudo-merohedral twins (incoherently twinned regular crystalline samples were already excluded because of the systematic extinctions observed) or random-tiling structures in the broadest sense of the word, also including crystalline microdomain structures with overall decagonal diffraction symmetry [*cf.* Figs. 1-4 of Welberry (1989)].

There is no way to distinguish between a quasicrystal and a high-order approximant within a given resolution. Thus, analysing the experimental data set by the *n*-dimensional approach one only fails if validity of the structural results is claimed for crystal parts larger than the respective experimental resolution (about 500 Å) allows. For the discussion of the structure in terms of coordination polyhedra, structure motifs and bond lengths this makes no difference. The same is true for the case of high-order approximant twinning discussed in the preceding paragraph.

In the case of any kind of random tiling-like structure (including coherent microdomain structures) an averaged quasiperiodic structure can be determined by an analysis neglecting diffuse scattering. In terms of the *n*-dimensional description, the *n*-dimensional unit cell of an average structure results from the superposition of all more or less differently occupied unit cells of the hypercrystal. Locally, such an average structure may look quite different from that which can be derived from an HRTEM image, for instance, since it reflects the global atomic distribution. As a result of averaging, distances between average atoms may be too small (split atoms). Consequently, constraints setting lower limits for possible interatomic distances must not be used in the refinements.

Least-squares refinements

A difficult problem in the course of the least-squares refinement of the five-dimensional structure model is the optimum parametrization of the two-dimensional perpendicular space components of the hyperatoms. In the case of the original Penrose tiling, for instance, these hyperfaces are represented by planar regular pentagons of well defined size with subregions corresponding to vertices of different types of coordination. Generally, the hyperfaces may have rather complicated shapes and fine chemical structure, especially in the presence of disorder, and each vertex type should be assigned a different temperature factor as is usual in the refinement of regular crystal structures. Because of the limited number N of observable reflections, however, the number n of variables must be kept small: a ratio N/n of at least 10 is recommended for standard structure determinations. A practical way out of this dilemma is to refine a rough structure model to an R factor smaller than ~0.15 for obtaining reliable phases for most of the structure amplitudes, and to work out the structural details employing the *n*-dimensional maximum-entropy method (MEM).

Maximum-entropy method

MEM principally represents a reconstruction technique giving the least-biased deduction compatible with given information. Applying this method to the problem of Fourier inversion, the best obtainable electron-density map can be derived from a noisy and/or incomplete set of diffraction data (*e.g.* Sakata & Sato, 1990, and references therein; Livesey & Skilling, 1985). In the usual method of Fourier transformation of the structure factors ('Fourier synthesis'), all non-observed structure factors are set to zero and series-truncation

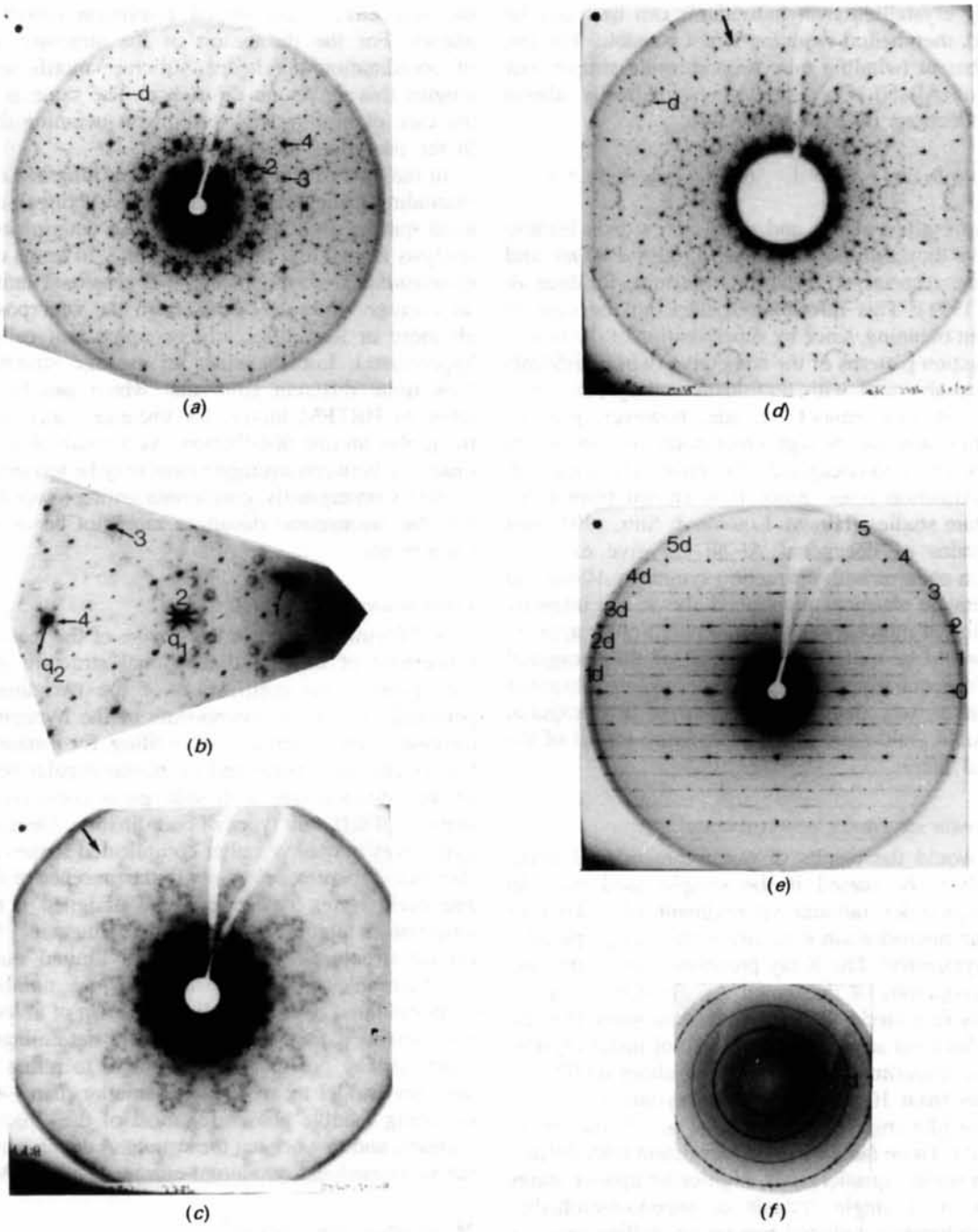

Fig. 1. X-ray precession photographs of decagonal $Al_{70}Ni_{15}Co_{15}$; all except (*e*) have plane symmetry 10*mm*. (*a*) Zero-layer photograph with the reflections 1 (10000), 2 (100$\bar{1}$0), 3 (110$\bar{1}$0), 4 (11$\bar{1}$1$\bar{1}$0) marked. Scattering phenomena belonging to the disordered superstructure system are indicated by *d*. On the high-resolution photograph (*b*) satellite reflections are visible around the reflections 1, 2, 3 and 4, for instance. One star of satellite vectors of length q_1 around 2 and one other vector of length q_2 pointing from reflection 4 to the centre of a diffuse pentagonal satellite cluster are marked by arrows. (*c*) The first diffuse layer belonging to the 8.08 Å superperiod. The structured diffuse scattering shows systematically extinct regions along the star of reciprocal basis vectors (shown by an arrow). (*d*) The first Bragg layer of the 4.04 Å period with systematic extinctions between the reciprocal basis vectors (shown by an arrow). The extinctions are partly superposed by the diffuse diffraction phenomena (indicated by *d*) of the superperiod. (*e*) The zero-layer photograph perpendicular to (*a*), clearly showing that the diffuse scattering (indicated by 1*d*, 2*d etc.*) is present in the Bragg layers (indicated by 0, 1 *etc.*), also. (*f*) The cone-axis photograph (*n*th Bragg-layer rings are indicated by 0 and 1, *n*th diffuse-layer rings by -1*d* and 1*d*), allows a comparison of the integral intensities of Bragg and diffuse scattering. [Mo $K\alpha$, Johansson-type focusing quartz monochromator, Rigaku RU 200 rotating-anode assembly, 0.3 × 0.3 mm^2 fine focus, 60 kV, 90 mA, μ = 30°, 60 mm crystal-to-film distance for (*a*), (*c*), (*d*) and (*e*), 100 mm for (*b*), and 30 mm for (*f*); 172 h exposure time for (*a*) and (*d*), 224 h for (*b*), 378 h for (*c*), 112 h for (*e*), and 5 h for (*f*).]

effects (ripples, dummy maxima and minima) appear in the electron-density maps. Thus, both observed and unobserved structure factors influence the results. MEM calculations, however, may be compared to constrained many-parameter least-squares refinements. A quasi-continuous electron density is modelled to obtain the best fit of calculated to observed structure factors. Another application of MEM, which was not used here, is the *ab initio* phase determination of structure factors (Bricogne & Gilmore, 1990). The first examples of MEM in the course of *n*-dimensional structure analyses of incommensurately modulated phases and decagonal quasicrystals were presented by Steurer (1992) and for the Fibonacci chain by Papoular, de Boissieu & Janot (1992).

In the present study MEM was employed following the five-dimensional least-squares refinements for obtaining high-quality electron-density maps of decagonal $Al_{70}Ni_{15}Co_{15}$. Since in our case of a centrosymmetric structure the phase problem was reduced to the sign problem, and the least-squares refinements yielded a final R factor significantly smaller than 0.1, it could be assumed that most of the signs obtained in this way were correct [the calculated signs were assigned to the observed structure amplitudes $|F_{obs}(\mathbf{H})|$] constituting a good MEM starting set.

For the calculations the Shannon/Jaynes configurational entropy

$$S = -\Sigma p_n(\mathbf{r})\ln[p_n(\mathbf{r})/p_{n-1}(\mathbf{r})],$$

with the probability $p_n(\mathbf{r}) = \rho(\mathbf{r})/\Sigma\rho(\mathbf{r})$, the prior probability $p_{n-1}(\mathbf{r}) = \tau(\mathbf{r})/\Sigma\tau(\mathbf{r})$, the electron density $\rho(\mathbf{r})$ and the prior electron density $\tau(\mathbf{r})$ at a particular pixel $\mathbf{r}$, was maximized under the constraint that the sum over the squared differences between observed and calculated structure factors becomes a minimum at the same time. The unconstrained maximization of S would result in a uniform electron-density distribution $\rho(\mathbf{r})$. Thus, using some approximations (Sakata & Sato, 1990) we get for the electron density

$$\rho(\mathbf{r}) = \tau(\mathbf{r})\exp\{2V\lambda\Sigma[F_{obs}(\mathbf{H}) - F_{calc}(\mathbf{H})] \times \cos(2\pi\mathbf{H}.\mathbf{r})/\sigma^2(\mathbf{H})\},$$

with a Lagrange multiplier λ and weights of the structure factors inversely proportional to their experimental variances $\sigma^2(\mathbf{H})$. The summation runs over all $\mathbf{H}$, the electron density $\rho(\mathbf{r})$ is given on a regular orthogonal grid defined in the physical space. The structure factors are calculated by Fourier transformation of the electron density

$$F_{calc}(\mathbf{H}) = 2V\Sigma\rho(\mathbf{r})\cos(2\pi\mathbf{H}.\mathbf{r})$$

summed up over half the grid points in the crystal volume V. Symmetry in direct and/or reciprocal space was taken into account. The iterations were started with uniform electron density on all grid points. For λ the maximum starting value giving convergence in the iterations was chosen by trial and error and optimized dynamically in the subsequent iteration cycles. The results were independent from the selected values. Values which were too small, however, needed a larger number of iterations to reach convergence.

The aim of the MEM calculations was to obtain large high-resolution density maps parallel to the physical space, and therewith an accurate representation of the quasiperiodic structure. By lifting the atoms in the embedding space, *i.e.* by assigning them all to a single five-dimensional unit cell, the shape of the hyperatoms parallel to the perpendicular space was reconstructed. Since no artifacts could be detected by visual inspection of the physical-space maps, the lift-density maps contain reliable information. In contrast the same sections calculated by Fourier synthesis are biased by truncation effects. Thus, the lifting process can be seen to act like a kind of noise filter.

The calculation of asymmetric units of physical-space electron-density maps was carried out on the following grids: 4000 × 4000 for a 190 × 190 Å^2 section of the density projected along the tenfold axis; 500 × 500 × 11 for a 95 × 95 × 1 Å^3 volume of the three-dimensional quasiperiodic structure. The computation time in the first case, using only $h_1h_2h_3h_40$ reflections, was about 2700 s for 17 iteration cycles, and in the second case, using all reflections, was 1800 s for 32 cycles on a Siemens S400/10 array processor. The electron density on the 4000 × 4000 grid was scanned by a peak-search program and the integrated densities above a given threshold value lifted into the five-dimensional unit cell giving the perpendicular space components of the five-dimensional hyperatoms.

Experimental

An alloy ingot with nominal composition $Al_{70}Ni_{15}Co_{15}$ was prepared by melting a mixture of Al (99.999%), Ni (99.98%) and Co (99.9%) in an induction furnace under Ar (99.999%) atmosphere. It was remelted under Ar and slowly cooled down (5 K min^{-1}) to room temperature. Subsequently, the sample was annealed at 1123 K for 1 d in an evacuated quartz ampulla and quenched in water. The ingot was crushed and several crystals with decaprismatic morphology were ground to spheres in a Bond chamber. An approximately spherical crystal with diameter 0.18 (2) mm was selected after checking by Laue photographs. The bulk density of the ingot was determined by displacement in CCl_4 to D_m = 4.17 (1) Mg m^{-3}. Since the samples contained cavities this value should rather be taken as a lower limit for the actual value which might be 5–10% higher. For comparison, the density of the monoclinic approximant

$Al_{13}Co_4$ (actually $Al_{74}Co_{26}$ according to the refined composition) was reported as D_m = 3.81 (5) Mg m^{-3} (Hudd & Taylor, 1962).

The data collection was performed on an Enraf–Nonius CAD-4 four-circle single-crystal diffractometer equipped with graphite monochromator (Mo $K\alpha$, λ = 0.70926 Å). In a first run a unique set of 4523 reflection intensities was collected within $0 < \theta < 45°$, the indices in the range $-6 < h_i < 6$, i = 1,..., 4, $0 < h_5 < 8$ and $|\mathbf{H}| \leq 2$ Å^{-1}. All reflections with intensities $I(\mathbf{H}) > 2\sigma[I(\mathbf{H})]$ were recollected within ten different asymmetric units to obtain better counting statistics and to minimize the influence of systematic errors by averaging. Thus, 5930 additional intensities were measured; the continuous 2.5% decay of the intensity-control reflection was corrected for, as well as the Lorentz and polarization effects. A spherical absorption correction was performed (minimum and maximum transmission factors 0.243 and 0.286, respectively); the linear absorption coefficient μ = 10.1 mm^{-1} was calculated from the mass absorption coefficients μ_k/ρ of the elements (*International Tables for X-ray Crystallography*, 1962, Vol. III). The corrected intensities were averaged yielding 556 unique reflections (R_i = 0.059); 253 reflections with $I(\mathbf{H}) > 2\sigma[I(\mathbf{H})]$ were used in the subsequent least-squares refinements and MEM calculations. Reflections with intensities $I(\mathbf{H}) \leq 2\sigma[I(\mathbf{H})]$, which are comparable to that of the underlying diffuse scattering, could not be separated adequately from the background and were rejected. The intensity distribution as a function of the perpendicular *versus* the parallel component of the diffraction vector $\mathbf{H} = (\mathbf{H}^{\parallel}, \mathbf{H}^{\perp})$ is illustrated in Fig. 2.

For the characterization of the quality of the single crystals and the exploration of the distribution of Bragg reflections and diffuse scattering numerous X-ray photographs (Fig. 1) were taken using the Buerger precession technique (for experimental details see figure captions). All precession photographs were over-exposed by at least a factor of 100 to visualize any weak diffraction phenomena like diffuse scattering, satellites or periodically arranged reflections in the case of approximants or twins. All Bragg reflections on the photographs except two types of satellite reflections can be indexed using the basis vectors $\mathbf{a}_i^*$, i = 1,..., 5. One set of satellites (Fig. 1*b*, labelled q_1) can be indexed by defining a star of satellite vectors $\mathbf{a}_i^{s*} = 0.124\mathbf{a}_i^*$, i = 1,..., 4; however, no satellites were included in data collection.

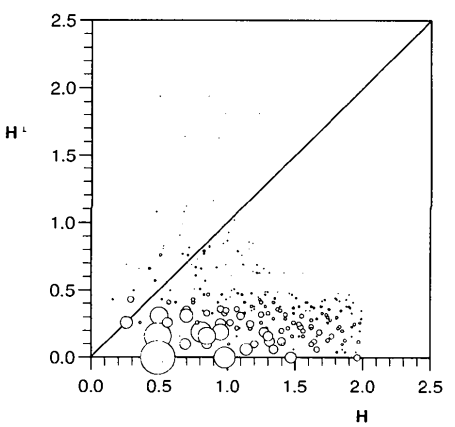

Fig. 2. Intensity statistics as a function of the perpendicular *versus* the parallel component of the diffraction vector $\mathbf{H} = (\mathbf{H}^{\parallel}, \mathbf{H}^{\perp})$. The radius of the circles is proportional to the respective structure amplitudes.

Diffuse interlayer lines on the precession photograph containing the tenfold axis (Fig. 1*e*) and on the cone axis photograph (Fig. 1*f*) indicate that the translation period perpendicular to the quasiperiodic layers (approximately 4 Å) has to be doubled. Similar diffuse diffraction phenomena, however, are also present in the layers of Bragg reflections masking the systematic absences ('between reciprocal basis vectors') of the reflections

$$h_1h_2\bar{h}_2\bar{h}_1h_5\text{: } h_5 = 2n + 1.$$

It is remarkable that for the diffuse scattering an extinction rule ('along reciprocal basis vectors') equivalent to that for the Bragg reflections is observed

$$h_10h_3h_3h_5\text{: } h_5 = 2n + 1$$

indicating the five-dimensional space groups $P10_5cm$ and $P10_5/mcm$, respectively, for the 8 Å superstructure. Thus, the set of c-glide planes present in the superstructure is rotated by $\pi/10$ with regard to the set of c-glide planes of the basic structure.

The second type of satellite reflections mentioned above is grouped in small pentagons with centres located on the same positions in the Bragg layers (Figs. 1*a* and 1*d*) as the diffuse maxima in the intermediate layers (Fig. 1*c*). Since the diffuse layers show reduced intensity at the positions of strong Bragg spots, one can conclude that these pentagonally clustered satellites belong to the 8 Å superstructure system. For a more detailed description of the diffuse-scattering phenomena see Frey & Steurer (1993).

Structure refinement and results

From the striking similarity between the X-ray diffraction patterns of decagonal $Al_{70}Ni_{15}Co_{15}$ and $Al_{65}Cu_{20}Co_{15}$ a close resemblance between their structures was expected. This was confirmed by the similarity of the characteristic sections of the respective five-dimensional Patterson functions [Fig. 3 of the present paper and Fig. 3 of paper (I)]. The least-squares refinements were performed starting with the five-dimensional structure model obtained for decagonal $Al_{65}Cu_{20}Co_{15}$. With some modifications

indicated by five-dimensional Fourier and difference Fourier syntheses, such as the decomposition of the hyperatoms 1 and 2 into partial hyperatoms 1′ and 1″, and 2′ and 2″, respectively, a model was derived which converged quickly to the final values $R = 0.091$ and $wR = 0.078$ for 21 refined parameters and 253 reflections. The high quality of the least-squares fit is illustrated in an $F_{obs}(\mathbf{H})/F_{calc}(\mathbf{H})$ plot (Fig. 4). Table 1 lists the 19 refined atomic parameters and those fixed.* The occupancy factor of hyperatom 3 was set to 1/2 because the short distance of 2.040 Å does not allow both the atomic sites in 00001/4 and 00003/4 to be occupied simultaneously. The occupancy factor of partial hyperatom 1′ was set to 1/2 because split atoms are generated by this area. Additionally, one scale factor and one empirical extinction factor g were refined $\{F^c_{calc}(\mathbf{H}) = F_{calc}(\mathbf{H})[1 - gF^2_{obs}(\mathbf{H})]/(\sin\theta/\lambda)\}$ which adopted a value of $g = 0.00058$ (6). Strong extinction effects for $0000h_5$ reflections could be expected since these reflections are very sharp. The reflection 00002, for instance, shows a full width at half maximum of only 0.012° corresponding to a coherence length of about 2500 Å (measured with synchrotron radiation on another crystal at HASYLAB/DESY with $\lambda = 0.9250$ Å). The stoichiometry of the single crystal used was not constrained in the refinements. However, the result came very close that of $Al_{69.6}Ni_{15.2}Co_{15.2}$ which is also very close to the nominal composition. Characteristic sections through the five-dimensional Fourier synthesis represent the distribution of the five-dimensional hyperatoms in the unit cell (Fig. 5) and their perpendicular space shape (Fig. 6). For comparison, the MEM high-resolution density maps obtained by the lifting method are also shown (Fig. 6). The peripheral parts of the hyperatoms with lower density correspond to the split atoms visible in the physical-space electron-density maps. The electron-density maps of the quasiperiodic layers in relation to the generation of five-dimensional hyperatoms are drawn in Fig. 7. The two typical in-plane atomic distances $d = 2.456$ Å (radius of a pentagon ≡ edge length of the corresponding Penrose unit tile) and $d = 2.887$ Å (edge length of the pentagons) are marked as well as typical split atoms which are interpreted in Fig. 12(*b*). In Fig. 7(*c*) the distance $d = 2.543$ Å between two atoms belonging to pentagonal structure units of adjacent layers is given. It is shorter than the in-plane bond with $d = 2.887$ Å. The highest maximum in the five-dimensional difference Fourier syntheses is about 2.6% of the highest maximum in the corresponding Fourier synthesis. The density of the final model, calculated from the least-squares fit parameter, amounts to $D_x = 4.5\ \mathrm{Mg\,m^{-3}}$ and is within the estimated density of 4.2–4.6 Mg m^{-3} The mean atomic volume of 13.5 Å^3 is smaller than that of monoclinic $Al_{13}Co_4$ with 14.2 Å^3 for fully occupied atomic sites (hypothetical case) and 15.6 Å^3 for the actual structure with partial occupation of particular positions. It is comparable, however, to the calculated density of $D_x = 4.4\ \mathrm{Mg\,m^{-3}}$ and the mean atomic volume of 13.8 Å^3 for hexagonal Co_2Al_5 (*i.e.* $Al_{71.4}Co_{28.6}$) (Newkirk, Black & Damjanovic, 1961). The mean atomic volume of 14.0 Å^3 and the density of

* A list of structure factors has been deposited with the British Library Document Supply Centre as Supplementary Publication No. SUP 71041 (3 pp.). Copies may be obtained through The Technical Editor, International Union of Crystallography, 5 Abbey Square, Chester CH1 2HU, England.

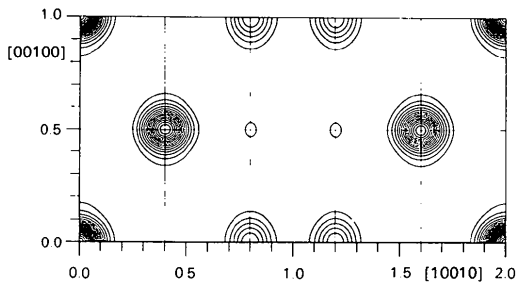

Fig. 3. Characteristic (10110) section of the five-dimensional Patterson function. All maxima of one five-dimensional unit cell are located on this special plane. All coordinates are given on the v basis.

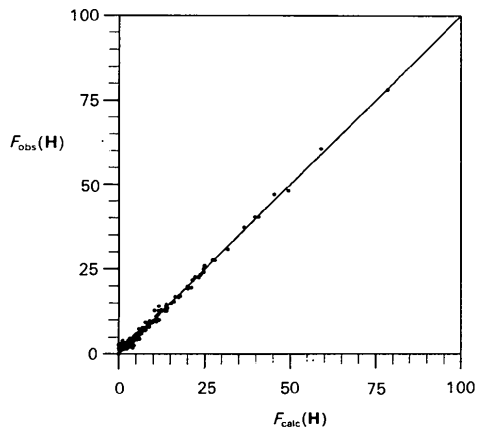

Fig. 4. $F_{obs}(\mathbf{H})/F_{calc}(\mathbf{H})$ plot for the final model.

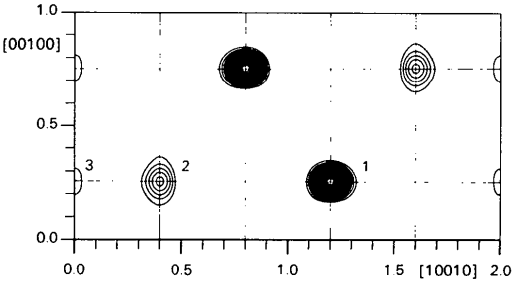

Fig. 5. (10110) sections of the five-dimensional Fourier function calculated after the last refinement cycle using $F_{obs}(\mathbf{H})$ for Fourier coefficients. The hyperatoms in the asymmetric unit are marked by 1, 2 and 3. All coordinates are given on the v basis.

4.3 Mg m^{-3} derived from the MEM maps are possibly more reliable than the values obtained from the fitted model parameters. In any case the density of the decagonal phase is significantly higher than that of its approximant phase, $Al_{13}Co_4$, indicating that the one type of quasiperiodic layer packing is more effective than the two types of periodic layer stacking of the approximant phase.

A comparison with the results of Yamamoto, Kato, Shibuya & Takeuchi (1990) is difficult: they used a

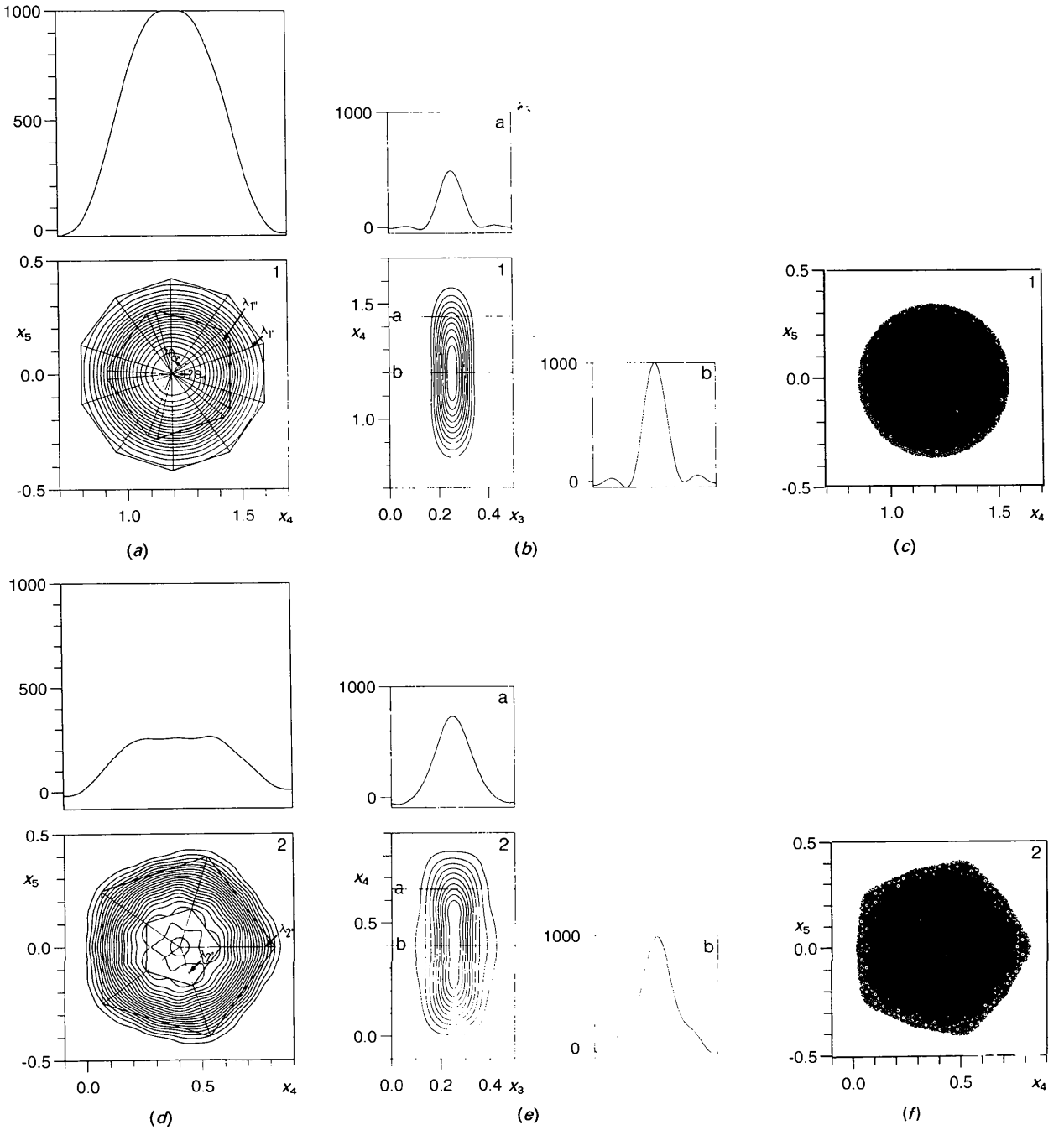

Fig. 6. Characteristic sections of the five-dimensional Fourier function: (*a*) perpendicular-space (00011) section of hyperatom 1 with polygon parameters for the partial hyperatoms 1′ and 1″ used in the refinements. The upper drawing gives the density along $x_5 = 0$. (*b*) (00110) section with densities along $x_4 = a$ and $x_4 = b$. (*c*) (00011) density distribution obtained by lifting the MEM results. In (*d*), (*e*) and (*f*) equivalent sections are displayed for hyperatom 2. All coordinates are given on the **v** basis.

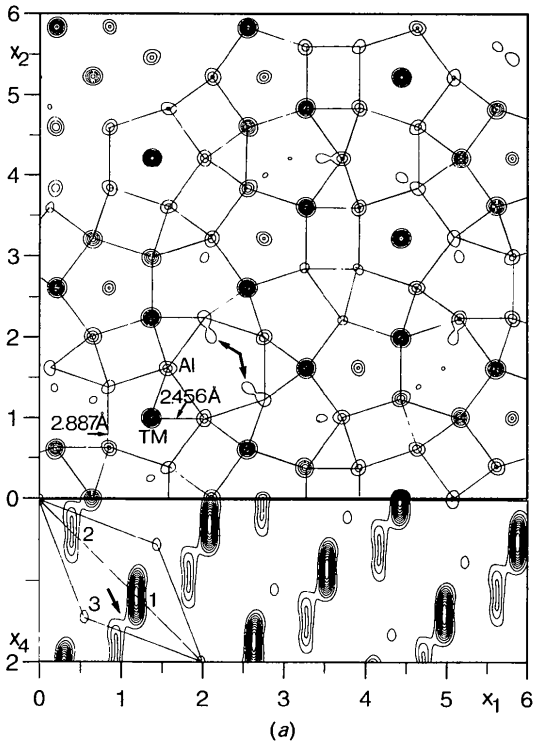

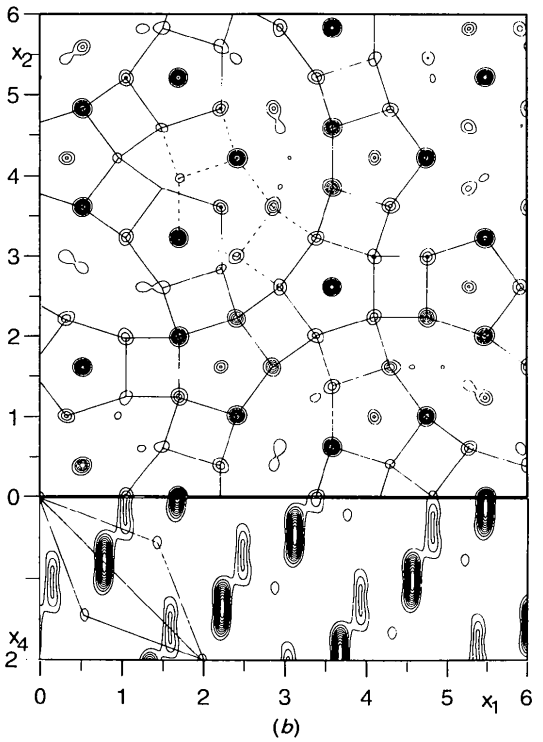

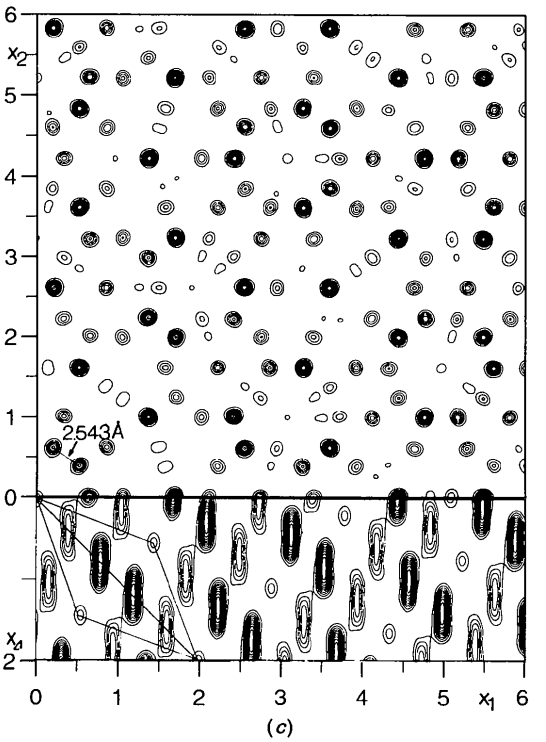

Fig. 7. 22.7 × 22.7 Å^2 parallel-space (11000) sections of the five-dimensional Fourier function at (*a*) $x_3 = 1/4$, (*b*) $x_3 = 3/4$ and (*c*) the projected structure. Additionally, the respective (10010) sections, with one unit cell drawn in and hyperatoms numbered, are shown to visualize the correspondence between five-dimensional and three-dimensional structure. One prominent structure motif, an icosagon formed by rectangles and pentagons, is drawn in (*a*) and (*b*). Two pairs of split atoms are marked by arrows in (*a*), the different pentagon–rectangle strips belonging to one pair of split atoms are shown in (*b*). All coordinates are given on the **v** basis.

crystal with nominal composition $Al_{70}Co_{20}Ni_{10}$, possibly located in the two- or three-phase region of the Al–Ni–Co phase diagram (Kek, 1991), with dimensions 0.2 × 0.2 × 3 mm and without applying any absorption correction; they included only the strongest 41 reflections in the refinements giving R = 0.11 as against our R = 0.03 for this subset. Thus, the information given in their paper is rather limited. Nevertheless, some rough similarities in the structure models can be found: the same special positions are occupied in the five-dimensional unit cell but the hyperatomic shapes are rather different, however.

Discussion

Packing and structure of the columns

The 190 × 190 Å^2 MEM electron-density map of $Al_{70}Ni_{15}Co_{15}$, a projection down the tenfold screw axis, displays characteristic large and small wheel-like motifs with decagonal symmetry completely covering the plane (Fig. 8). The large wheels appear to be packed in two ways: sharing one decagon edge with each other resulting in a distance S = 12.23(1) Å from centre to centre, or being bridged over two ~6 Å diameter disks leading to a distance $L = \tau S$ = 19.79 (1) Å (τ =

1.618..., - the golden mean). Frequently, the wheels are arranged in small or large pentagonal clusters with edge lengths S and L, respectively. The MEM density map shows a striking resemblance to HRTEM micrographs of $Al_{70}Ni_{15}Co_{15}$ annealed at 1073 K (Hiraga, Lincoln & Sun, 1991): the wheels in our map exactly correspond to the ring contrasts in the HRTEM structure images. By connecting the centres of these rings a quasiperiodic pentagon tiling can be obtained whereas for the sample annealed at 823 K a rhombic tiling with periodic regions (crystalline microdomains) results. Hiraga *et al.* interpreted the ring contrasts as caused by columnar clusters, and derived a structure model which is essentially compatible with our electron-density distribution (Figs. 7 and 8). A schematic drawing of the cross section of such a columnar cluster is shown in Fig. 9. Stacking these units alternately with units rotated $2\pi/10$ around the common fivefold axis, results in a columnar cluster with cylindrical symmetry $10_5/mmc$ and two-layer (~4 Å) periodicity, which consists of a central column surrounded by ten piles (its architecture is similar to the Greek kind of temple called *monopteros*). The central pentagons of the stacked layers form a pentagonal antiprismatic channel, its triangle faces being tesselated by slightly distorted tetrahedra (Fig. 10). The five empty peripheral pentagons of each structure unit are superposed by the five centred pentagons of the adjacent layers building ten pentagonal antiprismatic channels, but now only one half of the triangle faces are tesselated by tetrahedra. Each of the peripheral channels is linked to two neighbours *via* edge-sharing tetrahedra (Fig. 10). The dimensions of the pentagonal channels are, with a pentagon edge length of 2.887 (1) Å and a radius of 2.456 (1) Å, large enough to allow basic diffusion of atoms.

It is remarkable that the characteristic structure motif of the basic unit of the columnar clusters (*monopteros*), a strip of alternating pentagons and rectangles (marked in Fig. 9), is equivalent to the dominating element in the puckered y = 1/4 layer of the monoclinic approximant structure of $Al_{13}Co_4$ (Hudd & Taylor, 1962) (Fig. 11). This approximant layer consists of a wavy network of interpenetrating bands of alternating slightly distorted pentagons and rectangles with corners occupied by Al atoms, and the pentagons capped by Co atoms. The shuttle-like areas between the bands each contain one Al atom at adjoining corners of two equally sized distorted pentagons. In the basic unit of the columnar cluster (*monopteros*) the same shuttle-like areas can be found but now one of these pentagons becomes regular at the cost of the other replacing Al by TM (TM denotes transition metal, *i.e.* Ni/Co) atoms. It is noteworthy that the layers building the decagonal phase appear to be planar whereas the related atomic net of monoclinic $Al_{13}Co_4$ is puckered (~±0.3 Å). The projection of all the electron density on the tenfold axis, however, shows a density distribution with a large maximum centred at x_3 = 1/4 and small shoulders resulting from another underlying broader or double-peak distribution function centred also at x_3 = 1/4. This second distribution function

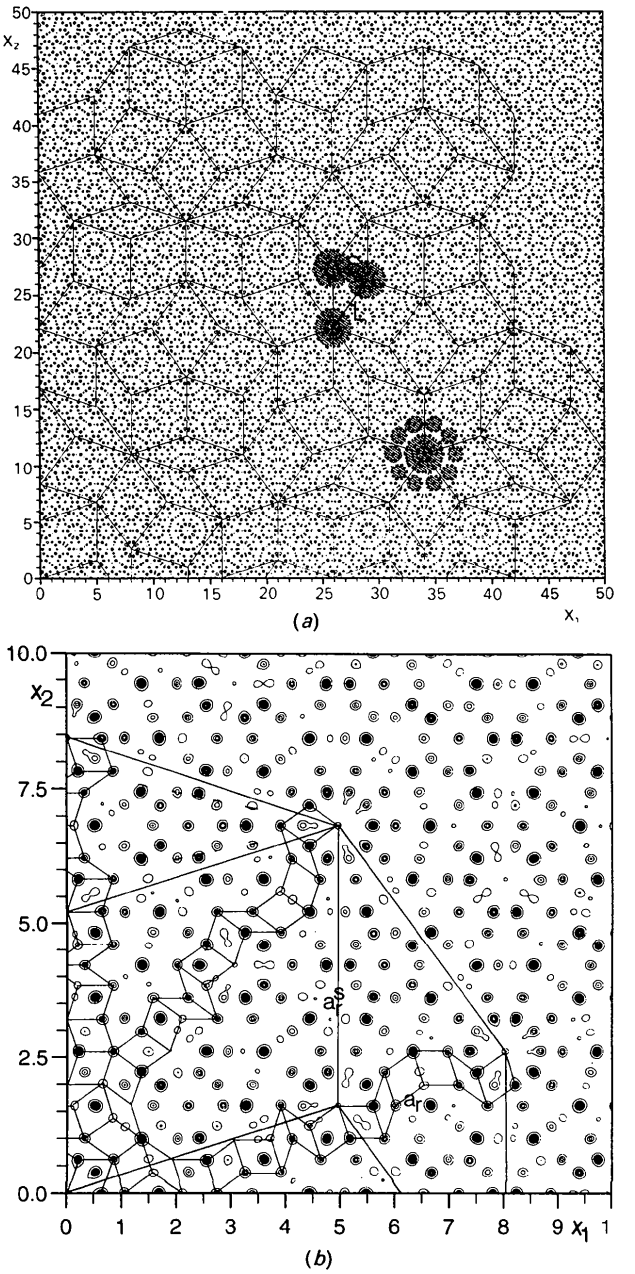

Fig. 8. Electron-density maps calculated by MEM. (a) 190 × 190 Å^2 parallel-space (11000) projection with super Penrose tiling drawn in, and distances S and L marked. One columnar cluster, consisting of a central column surrounded by ten piles (*monopteros*), is shaded. In (*b*) a magnified part of (*a*) is given to show the relationship between the basic Penrose tiling with edge length a_r = 2.456 (1) Å and the super Penrose tiling with $a_r^s = 2a_r(3\sin 2\pi/5 + 2\sin 2\pi/10)$ = 19.79 (1) Å. All coordinates are given on the ν basis.

indicates that a part of the atoms is located out of plane. Inspecting the (00110) sections of the five-dimensional Fourier syntheses of hyperatoms 1 and 2 (Figs. 6*b* and 6*e*) one finds that the density in the central part of hyperatom 2 is much more spread along x_3 than in those at the periphery (compare sections *a* and *b* of Fig. 6*e*). This finding is reflected in the values of the thermal parameters $B_{33}^{\parallel}$ of partial hyperatoms 2′ and 2″ (*cf.* Table 1), which correspond to r.m.s. displacements $\langle u^2\rangle^{1/2}$ = 0.3 Å for Al correlated with the central part compared to $\langle u^2\rangle^{1/2}$ = 0.2 Å for the others. It is not possible, however, to distinguish whether these values are related

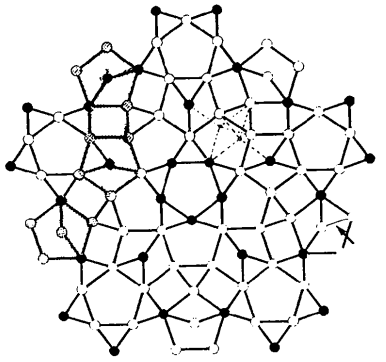

Fig. 9. Schematic drawing of the planar basic structural unit of a columnar cluster (*monopteros*). A crucial role is played by the triangle inside the decagons which can adopt three different equivalent positions as indicated. Open circles correspond to Al and closed circles to Ni/Co atoms. One of the pentagon-rectangle strips, an important structure motif, is shaded; one of the very short in-plane Al—Al distances is marked by an arrow.

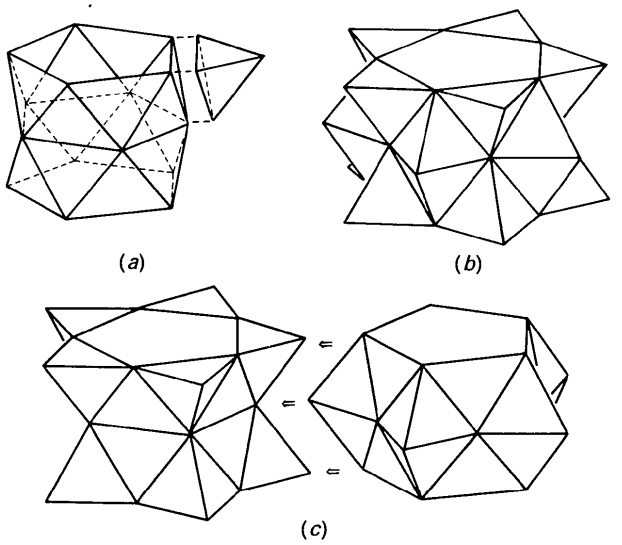

Fig. 10. (*a*) Schematic representation of the tessellation of the pentagonal antiprismatic channels with tetrahedra; (*b*) the central channel; (*c*) the peripheral channels are linked *via* edge sharing tetrahedra.

Table 1. *Parameters of the five-dimensional hyperatoms of decagonal* $Al_{70}Ni_{15}Co_{15}$ *with e.s.d.'s in parentheses*

The parameters listed are fractional hyperatomic coordinates x_i, i = 1,..., 4 (**d** basis); parallel-space temperature factors $B_1^{\parallel}$ isotropic in the quasiperiodic layers, and $B_{33}^{\parallel}$ perpendicular to them (Å^2); perpendicular-space temperature factor $B^{\perp}$ (Å^2); total site-occupancy factor p_k, partial site-occupancy factors p_{Al} and $p_{Ni/Co}$; radial hyperatomic size parameter λ_k as a fraction of a_i (a negative value denotes an opposite direction of $\lambda_k \mathbf{e}_i$); decagon parameter θ (rad). Hyperatom 1 of Fig. 5 is composed of the partial hyperatoms 1′ and 1″, hyperatom 2 of 2′ and 2″. All hyperatoms in the asymmetric unit are located at x_5 = 1/4 (**d** basis), have site symmetry 5*mm* and multiplicity 2.

Parameter	Hyperatom 1′	Hyperatom 1″	Hyperatom 2′	Hyperatom 2″	Hyperatom 3
x_i	2/5	2/5	4/5	4/5	0
$B_1^{\parallel}$	9(1)	1.19(5)	1.7(2)	2.9(5)	1(1)
$B_{33}^{\parallel}$	1.0(4)	0.57(5)	3.9(3)	7(1)	1(1)
$B^{\perp}$	0	0	1.7(4)	0	0
p_k	1/2	1	1	1	1/2
p_{Al}	0.94(10)	0	1	1	0
$p_{Ni/Co}$	0.06	1	0	0	1
λ_k	-0.42(1)	-0.29(2)	0.412(3)	0.18(3)	0.067(5)
θ	0.27(4)	0.07(9)	0	0	0

to thermal vibration or static positional disorder on the basis of our data. Since the central part of the hyperatoms generates fivefold coordinated vertices, the Al atoms centring the peripheral pentagons in Fig. 9 are those with the largest out-of-plane displacements. This is quite natural because the distance from these centring Al atoms to the Al atoms located at the corners of the pentagons in the adjacent layers below and above amounts to 3.193 Å, and the in-plane distance to the Al atom of the original pentagon is only 2.456 Å compared to the equilibrium Al—Al distance of 2.887 Å found in the other parts of the structure. If all centring Al atoms are displaced by x_3 = 1/4 (~1 Å) in the same direction the centred pentagonal antiprismatic channels could be described more accurately as a chain of cap-connected icosahedra. These correlated shifts of centring atoms may possibly cause disordering phenomena related to the diffuse scattering observed.

It is known from the study of the crystalline alloys in the binary systems Al-Ni and Al-Co that strong interactions between Al and TM exist as a result of electron transfer from Al to TM. Consequently, the resulting Al—Co distances are smaller than Al—Ni distances since Co, with one *d* electron less than Ni, is a stronger electron acceptor. That the same is true in the case of decagonal $Al_{70}Ni_{15}Co_{15}$ is suggested by the diamagnetic behaviour of this phase at room temperature which indicates completely filled *d* bands (Lück & Kek, 1993). Thus, covalent bonding as a result of hybridization effects between the TM *d* orbitals and the aluminium *s* and *p* orbitals may play a role in Al-TM compounds since, for instance, even in molten Al-Ni alloys the small mean atomic volume of 15.8 Å^3, compared to 18.8 Å^3 for a linear interpolation between the atomic volumes of the pure elements, indicates strong

interactions. The covalent bonding parts may favour planarity of the pentagon-rectangle strips.

In both Al-Ni and Al-Co binary systems metastable decagonal phases of approximate composition $Al_{75}Ni_{25}$ and $Al_{75}Co_{25}$ were detected whereas the $Al_{13}Fe_4$-type approximant only exists in the Al-Co system. The solubility of Ni in $Al_{13}Co_4$ is small whereas by substitution of Co by Ni in metastable decagonal $Al_{75}Co_{25}$ a stable decagonal phase can be produced. Thus, substitution of Co by Ni must influence the local coordination of this particular atom rather strongly. Looking at Fig. 9, one finds two types of TM coordination: TM centring Al pentagons is coordinated by five Al atoms in plane and $2 \times 3 = 6$ Al atoms in the adjacent layers; TM's at the corners of the peripheral pentagons are also surrounded by five Al atoms in plane but they form infinite TM-TM zigzag chains running in the periodic direction with TM of the neighbouring layers (d_{TM-TM} = 2.543 Å). Thus, accepting formal valencies of -0.61 for Ni, -1.71 for Co and +3 for Al (Raynor, 1949), Co is more likely to occupy the atomic sites surrounded completely by Al. This coordination-dependent distribution of Ni and Co may be one explanation for the stability of the ternary decagonal phase in contrast to the binary metastable phases.

From the inspection of the MEM density maps and the interpretation of the HRTEM structure images of the high- and the low-temperature phases (Hiraga, Lincoln & Sun, 1991), it is obvious that the columnar clusters (*monopteros*) represent the basic structural elements building the decagonal quasicrystal as well as the low-temperature microdomain structure. The preferred formation of columnar structure elements is also indicated by the columnar growth morphology of the decagonal phases: depending on the cooling rate, the needles reach length/diameter ratios of up to 100. For analysing the quasiperiodicity of the packing, the identification of a quasilattice (tiling) decorated with these columnar clusters would be very valuable. Thus, a natural choice for the edge length of a basic tile would be $a_r = L$, the distance between two columns. This would also be consistent with the distribution of ring contrasts in the HRTEM micrographs of both the high- and the low-temperature phase of $Al_{70}Ni_{15}Co_{15}$. In a Penrose tiling of this size drawn in the MEM map (Fig. 8) the wide rhombs appear to be decorated by columns on the vertices and on the long diagonals. There are no mistakes in the decoration of the vertices whereas in some cases the columns are flipped to the alternate positions on the long diagonals by reflecting through the short diagonal. These flips allow the formation of additional pentagonal clusters of columns with distance S from each other.

How arbitrary is the choice of a particular basic tile? This question is of interest since numerous theoretical models have been proposed with vastly differing unit-cell dimensions (Henley, 1993). Thus, an experimental finding uniquely fixing the edge length would be very valuable. One strong argument supporting our suggested tile size $a_r = L$ can be derived from the HRTEM findings (Hiraga, Lincoln & Sun, 1991): the packing of columns in the high- as well as in the low-temperature phase can be described by using the same wide and narrow rhombic unit tiles with $a_r = L$. The other strong argument is based on the interpretation of the X-ray diffraction patterns (Fig. 1): our indexing is related to an edge length of the rhombic unit tile a_r = 2.456(1) Å with an ambiguity of a factor τ^n (n = ..., -1, 0, 1, ...). The correspondence between a Penrose tiling based on such a small tile and our large tile is shown in Fig. 8(*b*). The vertices of the large tiling are a subset of those of the small one; they cannot be transformed into each other simply by scaling operations. Thus, the large tiling may be interpreted as a superstructure of the small one. The supercell is rotated by $\pi/10$ relative to the basic cell, *i.e.* as much as the set of *c*-glide planes of the two-layer structure is relative to that of the four-layer superstructure related to the diffuse-scattering phenomena (layers in Fig. 1*e*). The supercell results in the actual structure by the ordered occupation of one of the split positions (see Fig. 8*b*). Thus, if these considerations are correct superstructure reflections have to be observed. Indeed, the satellites, identified in Fig. 1(*b*) by vectors of length $a_i^s* = 0.124a_i*$, correspond exactly to a superstructure with edge length $a_r = L$ of the large unit tile. Fortunately, no ambiguity exists in the length of the satellite vector and the corresponding value for the edge length of the unit tile is fixed to $a_r = L$ = 19.79(1) Å which is consistent with the HRTEM findings.

Since we observe a Penrose tiling-like arrangement of columnar clusters, it might be possible to find local matching rules responsible for the quasiperiodicity,

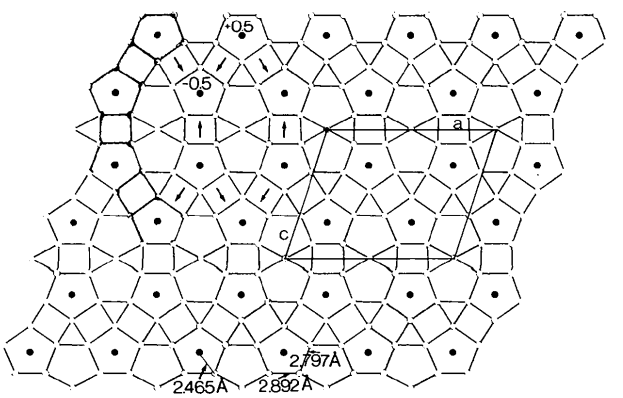

Fig. 11. Schematic representation of the puckered y = 1/4 layer of the monoclinic approximant $Al_{13}Co_4$. A characteristic subunit also occurring in the decagonal phase structure is shaded, the out-of-pentagonal plane deviations of capping Co atoms (closed circles) are given in Å. The arrows indicate the direction of increasing y parameter. One unit cell is drawn in.

explaining why the columns pack in a quasiperiodic manner. To this end, we discuss the scenario of how the clustering might occur: we start with one isolated column (*monopteros*) and connect it to a second one. The two columns, sharing two piles with each other, have a distance L and no atomic relaxation is necessary as a consequence of linking. The same consideration is valid for adding a third column (Fig. 12*a*) whereas the coupling of a fourth results in an ambiguity in the positions of two atoms per layer in the area common to two columns (marked in Fig. 12*b*). The centres of the four columns occupy the vertices of a wide rhombic tile with edge length $a_r = L$, with mirror symmetry around the short diagonal and a glide plane along the long diagonal. Removing the ambiguity by adopting one of the two possible atomic sites and slightly displacing one of the neighbouring atoms as indicated, a new column, with distance S to three other vertices and distance L to the far vertex, is generated on the long diagonal breaking the mirror symmetry of the rhombic tile. The short pentagon-rectangle strips which form a concave closed pentagonal band in the case of the isolated column are now connected to a nearly closed icosagonal ring. This icosagon can be closed by shifting two further atoms, and in the course of the continuing agglomerating process an extended network of closed icosagons is developed (Fig. 13). Under the assumption that the infinite pentagon-rectangle bands present in the approximant crystal $Al_{13}Co_4$ (Fig. 11) stabilize the monoclinic structure, the formation of an infinite network of these bands may also stabilize the quasiperiodic structure (resonance effect).

The structure of the layers

Let us now check the validity of the model discussed above by inspecting the electron-density maps of the quasiperiodic layers (Figs. 7 and 8). One notices, beside unequivocal electron-density maxima located on decagons and icosagons, numerous smeared and double peaks lying in between. These ambiguous peaks can be related to atoms shifted into either of the alternate positions during the relaxation of the four-column clusters forming the unit tile, since in the average structure all these different arrangements located in different parts of the crystal are projected onto each other. These alternate

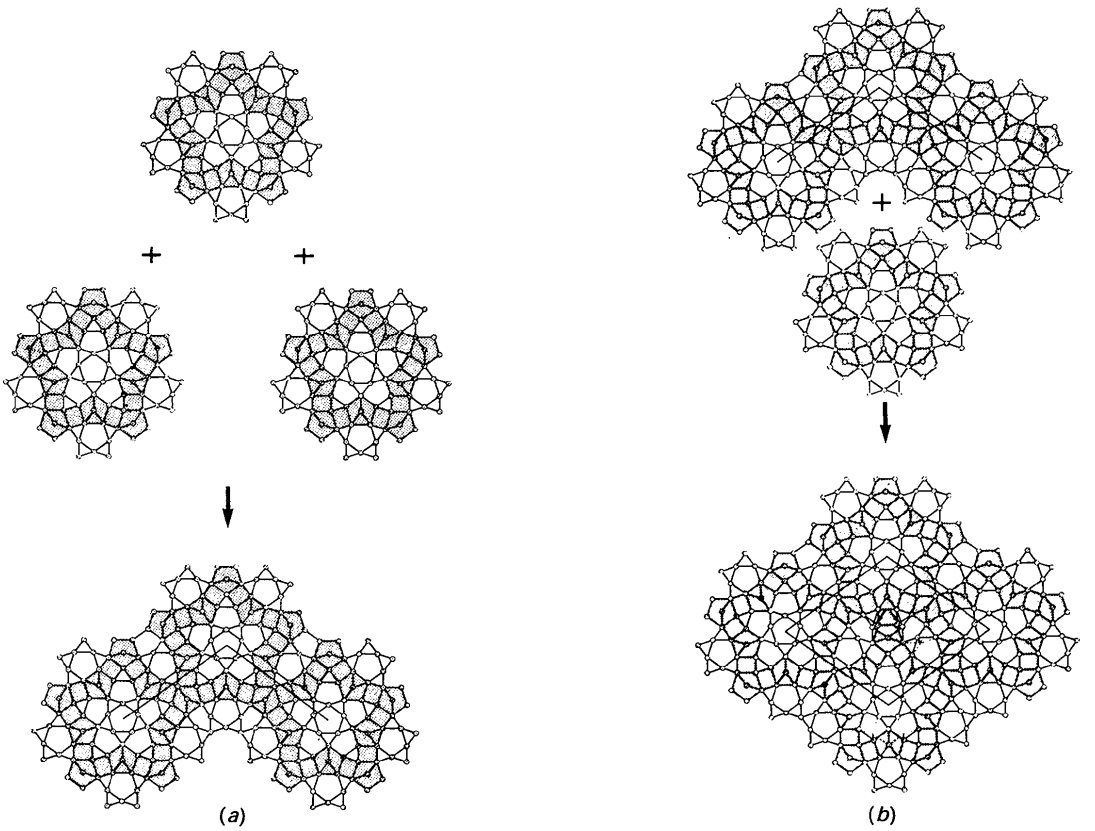

Fig. 12. Schematic scenario of the clustering process. (*a*) The linking of three columnar clusters (*monopteros*). The fourth cluster is connected in (*b*) leading to one pair of ambiguous atomic positions (marked by arrows). The icosagonal pentagon-rectangle ring can be closed by shifting two atoms (drawn with dotted lines and marked by small arrows).

arrangements may even be realized in different layers of each single wide unit tile, compensating in this way for the in-plane shifts forced by the clustering process by reversed shifts in the neighbouring double layers. This could also explain the existence of the 8 Å superperiod, and even its symmetry: the reflection plane relating the alternate positions in the average structure to each other would become a c-glide plane in the superstructure. The old glide plane, including an angle of $\pi/10$ with the new one, would vanish in the superstructure. Thus, the resulting stacking order of the 8 Å superstructure can be written in the form $AaA'a'$: A and a, as well as A' and a', respectively, are related by the c-glide plane with a glide component one layer up or down and direction 'between' the basis vectors; the c-glide plane relating A and A', as well as a and a', has a glide component two layers up or down and direction 'along' the basis vectors. Since the difference between the two enantiomorphic structures is small, the flip to the alternate position may occur many times during crystal growth eliminating mistakes in the quasiperiodic arrangement of tiles. These flips also allow a large number of combinations of the Y-like strips inside the closed icosagonal rings increasing the configurational entropy (Fig. 13). Thus, the vanishing of the structured diffuse scattering at high temperature may indicate a statistical distribution of these Y strips stabilizing the decagonal phase entropically. Lowering of temperature may force a more ordered antiphase arrangement of Y strips which is reflected in the diffuse scattering with systematic extinctions.

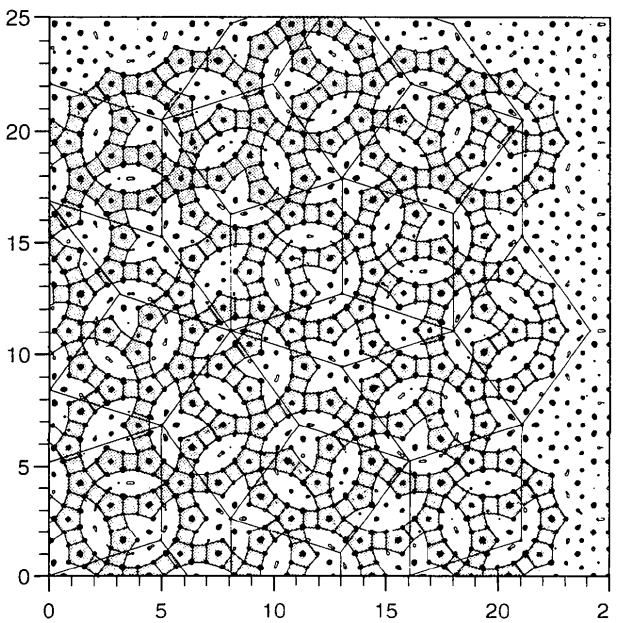

Fig. 13. 95 × 95 Å^2 parallel-space (11000) section at x_3 = 1/4 of the MEM electron-density map with the interconnected network of closed icosagonal rings and super Penrose tiling drawn in. The Y-like strips inside the closed rings may flip to alternate positions.

A glance at a 95 × 95 Å^2 MEM electron-density map of one layer (Fig. 13) reveals the complicated interconnected network of the pentagon-rectangle bands. Similar bands, as subsets of a Penrose tiling, have been predicted theoretically as main structure elements of decagonal phases by Kumar, Sahoo & Athithan (1986). A local matching rule can now be defined as an instruction to continue the strips ending at the edges of each unit tile in an appropriate way. It is not possible, however, to define two basic tiles invariably decorated with fragments of the strips. This decoration is context dependent. Certainly, this is only a weak local matching rule since rather long-range interactions are essential. It is also possible to build a periodic structure by packing the columns (Fig. 14) but impossible to obtain an interconnected network of closed icosagonal pentagon-rectangle rings. Closing of a ring in one unit cell opens the ring in the neighbouring unit cell. Thus, quasiperiodicity is a necessary condition for obtaining a network of closed rings.

Concluding remarks

A quantitative X-ray structure analysis was performed on a single crystal of decagonal $Al_{70}Ni_{15}Co_{15}$ using the higher-dimensional embedding method. The five-dimensional least-squares structure refinements were performed primarily to obtain phases for the structure factors, which are necessary to get a good start for the calculation of accurate electron-density distribution maps by the maximum-entropy method (MEM). From the maps columnar clusters were derived as basic structural units in accordance with HRTEM results. The quasiperiodic distribution of these columnar clusters was interpreted in terms of a super Penrose tiling with dimensions of the basic rhombs fixed by the satellite vector. This tiling shows a context-dependent decoration

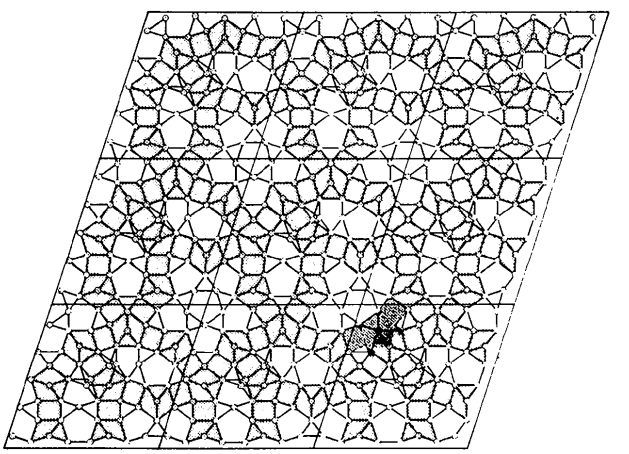

Fig. 14. Schematic representation of a periodic structure built from the wide rhombs of the super Penrose tiling. The closing of one icosagon opens another one in the neighbouring unit cell (marked on the lower right-hand side).

with pentagon–rectangle strips leading to an interconnected infinite network; the same bands can be found in the approximant structure of $Al_{13}Co_4$ connected to periodic nets. Quasiperiodicity, however, is a necessary prerequisite for the existence of an infinite network of interconnected *closed* icosagonal rings.

This work was supported by DFG Ste581/1-1.

References

ARAKI, T. (1991). *Z. Kristallogr.* **194**, 161-191.

BEELI, C., NISSEN, H.-U. & ROBADEY, J. (1991). *Philos. Mag. Lett.* **63**, 87-95.

BRICOGNE, G. & GILMORE, C. J. (1990). *Acta Cryst.* A**46**, 284-297.

BURKOV, S. E. (1991). *Phys. Rev. Lett.* **67**, 614-617.

DAULTON, T. L. & KELTON, K. F. (1992). *Philos. Mag.* B**66**, 37-61.

EDAGAWA, K., ICHIHARA, M., SUZUKI, K. & TAKEUCHI, S. (1992*a*). *Philos. Mag. Lett.* **66**, 19-25.

EDAGAWA, K., ICHIHARA, M., SUZUKI, K. & TAKEUCHI, S. (1992*b*). *Tech. Rep. ISSP* A2530.

FREY, F. & STEURER, W. (1993). *J. Non Cryst. Solids*, **153/154**, 600-605.

FUNG, K. K., ZOU, X. D. & YANG, C. Y. (1987). *Philos. Mag. Lett.* **55**, 27-32.

GRUSHKO, B. (1993). *Phase Transit.* In the press.

HE, L. X, ZHANG, Z., WU, Y. K. & KUO, K. H. (1988). *Inst. Phys. Conf. Ser.* **93**, 501-502.

HENLEY, C. L. (1993). *J. Non Cryst. Solids*, **153/154**, 172-176.

HIRAGA, K., LINCOLN, F. J. & SUN, W. (1991). *Mater. Trans.* **32**, 308-314.

HUDD, R. C. & TAYLOR, W. H. (1962). *Acta Cryst.* **15**, 441-442.

INOUE, A., TSAI, A. P. & MASUMOTO, T. (1990). *Quasicrystals, Springer Series in Solid State Science*, Vol. 93, edited by T. FUJIWARA & T. OGAWA, pp. 80-93. Berlin: Springer-Verlag.

JANSSEN, T. (1988). *Phys. Rep.* **168**, 55-113.

KANG, S. S. & DUBOIS, J. M. (1993). *Phase Transit.* In the press.

KEK, S. (1991). Thesis, Univ. Stuttgart, Germany.

KUMAR, V., SAHOO, D. & ATHITHAN, G. (1986). *Phys. Rev. B*, **34**, 6924-6932.

LIVESEY, A. K. & SKILLING, J. (1985). *Acta Cryst.* A**41**, 113-122.

LÜCK, R. & KEK, S. (1993). *J. Non Cryst. Solids*, **153/154**, 329-333.

NEWKIRK, J. B., BLACK, P. J. & DAMJANOVIC, A. (1961). *Acta Cryst.* **14**, 532-533.

PAPOULAR, R. J., DE BOISSIEU, M. & JANOT, C. (1992). *Methods of Structural Analysis of Modulated Structures and Quasicrystals*, edited by J. M. PEREZ-MATO, F. J. ZUÑIGA & G. MADRIAGA, pp. 333-343. Singapore: World Scientific.

RABSON, D. A., MERMIN, N. D., ROKHSAR, D. S. & WRIGHT, D. C. (1991). *Rev. Mod. Phys.* **63**, 699-733.

RAYNOR, G. V. (1949). *Prog. Met. Phys.* **1**, 1-76.

SAKATA, M. & SATO, M. (1990). *Acta Cryst.* A**46**, 263-270.

SONG, S. & RYBA, E. R. (1992). *Philos. Mag. Lett.* **65**, 85-93.

SONG, S., WANG, L. & RYBA, E. R. (1991). *Philos. Mag. Lett.* **63**, 335-344.

STEURER, W. (1991). *J. Phys.* **3**, 3397-3410.

STEURER, W. (1992). *Methods of Structural Analysis of Modulated Structures and Quasicrystals*, edited by J. M. PEREZ-MATO, F. J. ZUÑIGA & G. MADRIAGA, pp. 344-349. Singapore: World Scientific.

STEURER, W. (1993). *J. Non Cryst. Solids*, **153/154**, 92-97.

STEURER, W. & KUO, K. H. (1990). *Acta Cryst.* B**46**, 703-712.

TSAI, A. P., INOUE, A. & MASUMOTO, T. (1989). *Mater. Trans.* **30**, 463-473.

TSAI, A. P., INOUE, A. & MASUMOTO, T. (1991). *Philos. Mag. Lett.* **64**, 163-167.

WELBERRY, R. T. (1989). *J. Appl. Cryst.* **22**, 308-314.

YAMAMOTO, A., KATO, K., SHIBUYA, T. & TAKEUCHI, S. (1990). *Phys. Rev. Lett.* **65**, 1603-1606.

YAN, Y., WANG, R., GUI, J., DAI, M. & HE, L. (1992). *Philos. Mag. Lett.* **65**, 33-41.

Acta Cryst. (1993). B**49**, 675–679

Structure of Disodium Monocalcium Tartrate Monosuccinate Trihydrate, $Na_2(CaTMS).3H_2O$

BY THOMAS J. EMGE,* JOEL D. OLIVER, DANIEL S. CONNOR AND SUSAN M. THOMAN

The Procter and Gamble Company, Miami Valley Laboratories, Cincinnati, Ohio 45239-8707, *USA*

AND MARK E. JASON

The Monsanto Chemical Company, St Louis, Missouri 63167, *USA*

(*Received* 3 *September* 1992; *accepted* 18 *January* 1993)

Abstract

Crystals of disodium monocalcium tartrate monosuccinate (TMS) trihydrate, $Na_2Ca(C_8H_6O_{10}).3H_2O$, M_r = 402.2, are monoclinic, space group $P2_1/n$ with a = 7.989(1), b = 16.543(2), c = 11.416(1) Å, β = 106.48(1)°, V = 1446.8(6) Å^3, Z = 4, D_x = 1.846 Mg m^{-3}, λ(Mo $K\alpha$) = 0.71069 Å, μ(Mo $K\alpha$) = 0.55 mm^{-1} and $F(000)$ = 824. X-ray intensity data for 3337 independent reflections with $F > 4\sigma(F)$ and $2\theta < 60°$ were measured. The structure was refined to $R(F)$ = 0.031. The crystalline phase studied here is the sodium salt of a $Ca(TMS)^{2-}$ complex, with edge-bridged trigonal bipyramidal and octahedral geometries for the Na^+ ions and a dodecahedral geometry for the eight-coordinate Ca^{2+} ion. The O atoms from the ether moiety and three carboxylate groups of the TMS anion participate in a tetradentate binding to the Ca^{2+} ion. The α-hydroxycarboxylate group of the tartrato portion of the anion exhibits bidentate binding to the Ca^{2+} ion and one carboxylate group serves as a bidentate chelate

* Current affiliation: Chemistry Department, Wright-Rieman Laboratories, Rutgers University, Piscataway, NJ 08855-0939, USA.